Computers in Biology and Medicine 109 (2019) 62–69

Contents lists available at ScienceDirect

Computers in Biology and Medicine

journal homepage: www.elsevier.com/locate/compbiomed

Effect of scaffold architecture on cell seeding efficiency: A discrete phase model CFD analysis

Davar Ali[a,b,*]

[a]Hacettepe University, Faculty of Engineering, Department of Chemical Engineering, Ankara, Turkey
[b]Karabuk University, Faculty of Engineering, Department of Medical Engineering, Karabuk, Turkey

ARTICLE INFO

Keywords:
Cell culture efficiency
TPMS scaffolds
CFD analysis
Discrete phase modeling

ABSTRACT

Within perfusion cell culture systems, scaffold architecture is able to control important biological parameters such as permeability and fluid flow-induced shear stress. As well, one of the main factors affecting the final fate of this process as well as optimal cell differentiation and proliferation in these systems is initial adhesion of cells to scaffolds. In this study, the effect of scaffold architecture on the adhesion of the cells was computationally investigated. For this purpose, four scaffold models including double-diamond, gyroid, FR-D, and Schwarz-primitive were designed using triply periodic minimal surface (TPMS) geometry with a constant porosity of 80%. As well, the inlet velocity of zero to simulate static cell culture and three different inlet velocities for modeling the dynamic cell culture conditions were also selected. The results showed that cell culture efficiency of scaffolds could be changed up to seven times from architecture to architecture under the same conditions. The efficiency of cell culture in scaffolds with tortuous architecture was also reported higher than those with relatively straight microchannels. In terms of culture methods, unlike dynamic cell culture model in which almost a homogeneous cell distribution was observed in static cell culture simulation, more cells adhered, but they had agglomerated in the scaffold entrance regions and had failed to reach all regions. The results of this study shed more light on the selection and design of scaffold architecture for optimal cell culture in tissue engineering.

1. Introduction

Cell therapy is known as an effective method to accelerate treatments of lesions in organs that have lost their functions. Accordingly, patients' cells are cultured within an appropriate scaffold and then transplanted into target tissues [1]. Use of perfusion bioreactors is similarly considered as a promising method that is widely utilized in stem cell culture to synthetize scaffolds [2]. Diffusion, proliferation and differentiation of stem cells within the pores of a scaffold can be further affected by numerous parameters. Nevertheless, an initial adhesion of cells to scaffolds to initiate proliferation and differentiation of such cells during cell culture is essential [3]. Although use of perfusion bioreactors ensures penetration of cells into scaffold channels, cell adhesion and placement on scaffold walls are dependent on many factors such as material properties including surface topography, surface chemistry, wettability, and elastic modulus [4–7].

Various studies have been conducted to investigate the effect of geometrical parameters on adhesion of cells to scaffolds [3,8]. In this respect, Murphy et al. reported that the maximum number of initial cell adhesions could happen in scaffolds with a pore size of 120 μm [9]. In a perfusion cell seeding, distribution and adhesion of cells was also studied by Melchels et al. According to their results, the highest cell density was observed in areas with the largest pores and the highest fluid velocities [10]. Bael et al. also examined the effect of pore geometry on biological behaviors of human periosteum-derived cells cultured on additively- manufactured bone scaffolds. Their findings in this domain indicated that although scaffolds with smaller pores had promoted more initially cell adhesions, they had caused occlusion and consequently decreased the permeability of scaffolds [11]. Based on these studies and their conflicting results, it could be concluded that no optimal design of scaffolds for cell culture had been previously presented. Therefore, more studies were required to better understand movements and depositions of cells on scaffolds.

It should be noted that in vitro studies of cell culture on scaffolds are time-consuming and costly. Moreover, scaffolds are often made up of opaque materials and thus having access to their inner parts to visualize motions and behaviors of the cells within scaffold pores is not a straightforward task [12]. Recently, a pre-assessment of optimal designs for the scaffolds in silico models has been proposed as a promising tool to overcome these difficulties [13–17]. For example, Marin et al.

* Hacettepe University, Faculty of Engineering, Department of Chemical Engineering, Ankara, Turkey.
E-mail address: daverali@atauni.edu.tr.

https://doi.org/10.1016/j.compbiomed.2019.04.025
Received 4 February 2019; Received in revised form 20 April 2019; Accepted 20 April 2019

examined cell motions within scaffolds using experimental (μ-Particle tracking velocimetry) and a multiphase-based computational fluid dynamics (CFD) analysis and found that cells had pursued fluid streamlines in the scaffolds in both experimental and CFD analyses [18]. In another work, they probed cell streamlines within scaffold pores in a perfusion cell culture system using computational discrete phase models (DPMs) and reported that the flow rate had played a prominent role in cell deposition on scaffold walls [19]. Although their studies showed the eligibility of CFD analysis to simulate the dynamics of cells within scaffolds, they used only a simple architecture of bone scaffolds whereas more sophisticated architectures could be exploited in such designs [20,21]. The effects of scaffold geometry parameters on fluid dynamics within them were also reported in various studies [22–24]. Therefore, it is expected that scaffold architecture play an important role in adhesion of cells to scaffold microchannels.

To understand the effect of scaffold architecture on cell seeding efficiency in a perfusion cell culture system, four different scaffolds with a constant porosity of 80% were designed using TPMS in this study. Cell movements were also simulated via a DPM computationally. The cells were seeded at four different flow rates and cell seeding efficiency in each model was assessed as the percentage of deposited cells to the whole number of injected ones.

2. Materials and methods

2.1. Scaffold models

Four TPMS scaffolds including double-diamond [25], gyroid [20], F-RD [26], and Schwarz-primitive [27] were designed. The primary surfaces of the scaffolds were also created using the K3Dsurf (k3dsurf.sourceforge.net) software. Then, the obtained surfaces in mesh file extension of .obj were imported into the SolidWorks software and were thickened to obtain the desired porosity. A wall thickness of 100 μm, producible by additive manufacturing method, was also selected for the scaffolds [28,29]. Trigonometric functions of x, y, and z used in building the TPMS scaffold structures were presented in Table 1.

Repeating unit cells by four times in three axes (x, y, and z) provided a cube model with 64 unit cells for each scaffold. The fluid domains of the models were also obtained by subtracting the solid domains from an enclosing box. Unit cells of models and their geometrical parameters with the corresponding solid and fluid domains were presented in Fig. 1 and Table 2.

In this study, all the four unit cells exploited were isometric and had the same architecture in three axes (x, y, and z). The geometrical parameters of the unit cells were listed in Table 2.

2.2. Governing equations in continuous phase

Navier-Stokes equation was used in the CFD analysis to examine a fully developed and laminar flow of an incompressible fluid with a constant density and viscosity [30]:

$$\rho\frac{\partial \mathbf{u}}{\partial t} - \mu\nabla^2\mathbf{u} + \rho(\mathbf{u}.\nabla)\mathbf{u} + \nabla p = \mathbf{F}, \quad \nabla.\mathbf{u} = 0 \tag{1}$$

Wherein; ρ, **u**, and μ respectively denoted density (1000 kg/m3 [31]), velocity (m/s), and fluid dynamic viscosity (Pa.s). As well, ∇ and p respectively represented del operator and pressure (Pa). Finally, **F** indicated forces such as gravity and centrifugal force, where **F** = 0 in the present study [30,32].

Table 1
Parametric equations for TPMS structures.

TPMS architecture	Equations f (x,y,z) = 0
Double diamond	$\cos(x)\cdot\cos(y)\cdot\cos(z)-\sin(x)\cdot\sin(y)\cdot\sin(z)$
Gyroid	$\cos(x)\cdot\sin(y)+\cos(y)\cdot\sin(z)+\cos(z)\cdot\sin(x)$
F-RD	$3(\cos(x)+\cos(y)+\cos(z))+ 8(\cos(x).\cos(y).\cos(z))$
Schwarz-primitive	$\cos(x)+\cos(y)+\cos(z)$

2.3. Governing equations in discrete phase

Considering the cells as particles, their motions within scaffold channels could be explained using particle motion equation [33], which was defined by the following equations:

$$\frac{dU_P}{dt} = f_d\,(U - U_P) + \frac{g\,(\rho_P - \rho)}{\rho_P} \tag{2}$$

and;

$$f_d = \frac{18\mu}{\rho_P d_P^2}\frac{C_d Re}{24} \tag{3}$$

wherein; U_P, f_d, U, g, ρ_p, ρ, μ, d_P, C_d, and Re represented particle velocity (m/s), drag force (N), fluid phase velocity (m/s), gravitational acceleration (9.81 m/s^2), cell density (1130 kg/m^3 [34]), fluid density (1000 kg/m3 [31]), fluid dynamic viscosity (0.001 Pa s [35]), cell diameter (10 μm [13]), an empirical drag coefficient factor for spherically-shaped particles [33] and Reynold's number respectively.

To probe whether the particles had followed a carrier fluid streamline or not, the Stokes number was calculated as [18,36]:

$$Stk = \frac{\rho_p d_P^2 V}{18\mu\chi} \tag{4}$$

Wherein ρ_p and d_P referred to cell density and diameter, V denoted average velocity of fluid, μ showed fluid dynamic viscosity, and χ was particle dynamic shape factor (where the cell assumed to be spherical particles the χ has a magnitude of 1 [37]). In this study, a Stk«1 indicated that the cells had followed fluid streamlines.

2.4. Boundary conditions

Using tetrahedral elements, the scaffold geometries were meshed [38,39] with maximum mesh size of 30 μm (Fig. 2). A steady-state and laminar flow was exploited to simulate the culture medium flow. Four velocities of 0.001, 0.0005, 0.0001 and 0 m/s were correspondingly assigned to the inlet, where the latter (0 m/s) showed a static cell culture state and the media did not flow.

In this study a maximum Reynolds number of 10.16 indicates that analysis took place in a laminar flow (Table 3). The output pressure was also selected as zero and the scaffold wall was assumed to be hydrophilic. Then, a no-slip boundary condition was imposed to the scaffolds walls [35].

The cells were also modeled as spherical discrete phase with a diameter of 10 μm and density of 1130 kg/m3 [13]. Moreover, one-way coupling was considered between cells and media, so that only fluid phase was able to affect the cells. After that, the cells were injected from the inlet surface with a zero velocity [18]. A cell density of 10^6 cells/mL in the media was also selected [40]. To simplify the analysis, a uniform distribution of the cells in the fluid phase was assumed, so that one cell was assigned in the inlet surfaces for any 100 × 100 μm^2 area (Fig. 3). Ansys Fluent software was used to solve the equations of DPMs.

It was assumed that the cells adhered to the scaffold walls had once collided with it. To this end, wall interaction with the discrete phase cells was assigned as the trap condition [13].

3. Results

3.1. Mesh dependency analysis

In the previous DPM studies, it was reported that particles trajectory and their final fate were highly dependent on the mesh quality of fluid phase [39,41]. Therefore, to probe the mesh quality impact on cell

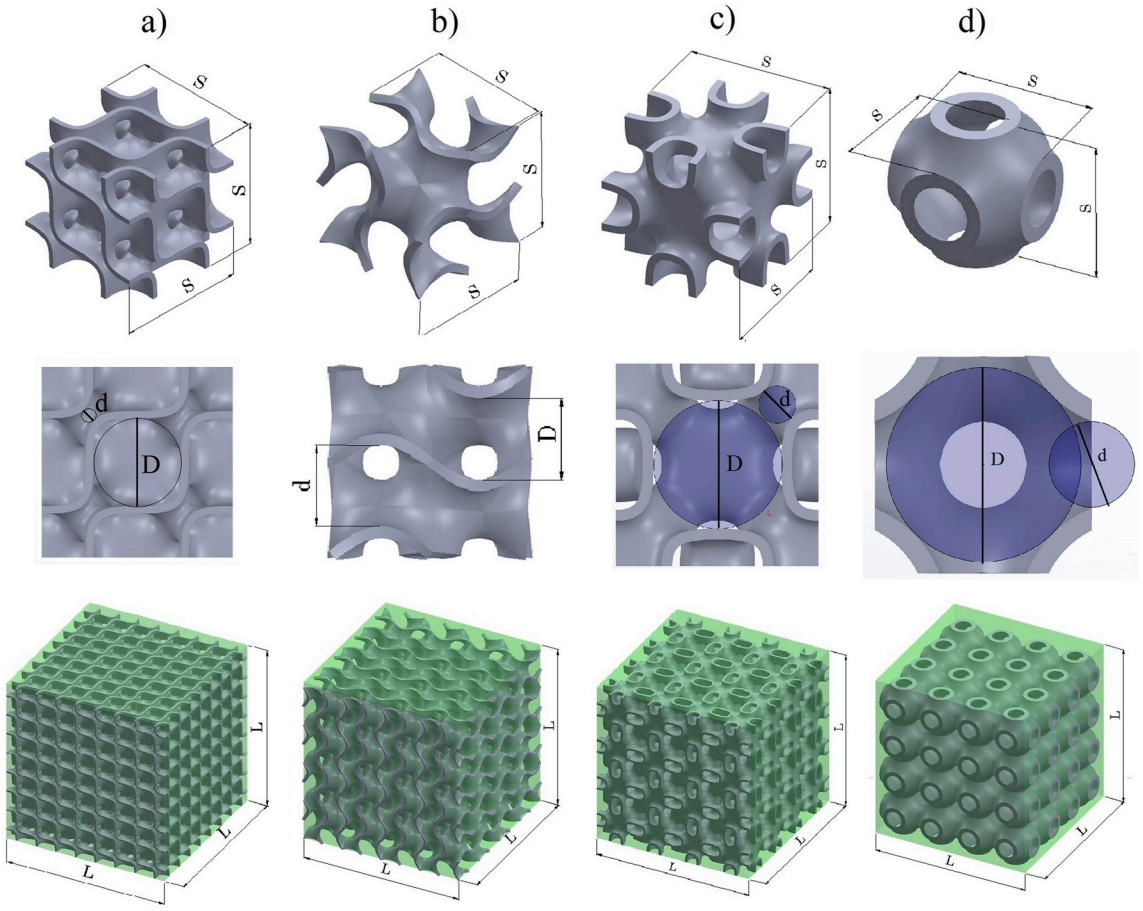

Fig. 1. Unit cells in their cross-section view and related three-dimensional (3D) scaffolds with solid (gray) and fluid (green) domains; a) double-diamond, b) gyroid, c) FR-D, and d) Schwarz-primitive.

Table 2
Geometrical parameters of scaffolds; in which, L, s, D, and d respectively denoted sizes of the models, length of unit cells, as well as the widest and the narrowest sizes of the pores.

Model parameters	TPMS scaffolds Length in x, y, z calculated in the $[-\pi, \pi]$ boundary			
	Double-diamond	Gyroid	F-RD	Schwarz-primitive
L (mm)	10.16	6.24	7.36	4.00
s (mm)	2.54	1.56	1.84	1.00
D (mm)	1.17	0.68	1.17	0.90
d (mm)	0.20	0.68	0.39	0.40

deposition the sensitivity of trapped cell number to mesh size was conducted for each model (Fig. 4).

Reducing mesh size caused decrease in deposited cells number in all the models. A mesh size of 30 μm left us approximately element numbers of 47, 31, 23 and 19 million for double-diamond, gyroid, FR-D, and Schwarz-primitive models respectively. It is worth noting, that achieve an excellent convergence for DPM was not affordable with available computational facilities. However, there was only a minor deviation in trapped cell number for mesh sizes of 35 and 30 μm in all models. Therefore, in this study models were analysed with a maximum mesh size of 30 μm.

3.2. Fluid dynamics within scaffolds

To understand the fluid flow modality within scaffolds, plot of velocity contour of each model was illustrated in Fig. 5.

Fig. 5 shows that fluid velocity within scaffold pores is variable and in the obstructed area, its magnitude is higher than in wider areas. This change in velocity magnitude is more pronounced in the double-diamond model. Because according to Table 2 this model has the highest ratio of D/d.

3.3. Cells trajectory

As discussed in 2.3 section a Stk«1 can assure us that cells will follow fluid domain streamlines. Fig. 6 shows the fluid velocity streamlines and cells trajectories in the model corners. As shown in this Figure, cells trajectories roughly corresponded to fluid domain streamlines. Such similarity in particle trajectories and fluid velocity streamlines also was reported in the work of Marin et al. [18].

3.4. Effect of flow rate on cell sedimentation

Considering the inlet area of the models, the number of cells for injection was also calculated as 10322, 3893, 5225 and 1600 for double-diamond, gyroid, F-RD, and Schwarz-primitive models; respectively. The trapped cell number for each model at the selected inlet velocity was shown in Table 4.

Through varying scaffold architecture and inlet velocity, a dramatic change was observed in the percentage of the trapped cells (Fig. 7).

As expected, the percentage of trapped cells increased in all models as the inlet velocity dropped. This trend complies with the work results of Marin et al. [19]. Among the models, the double-diamond one showed the highest amount of deposited cells for all inlet velocities

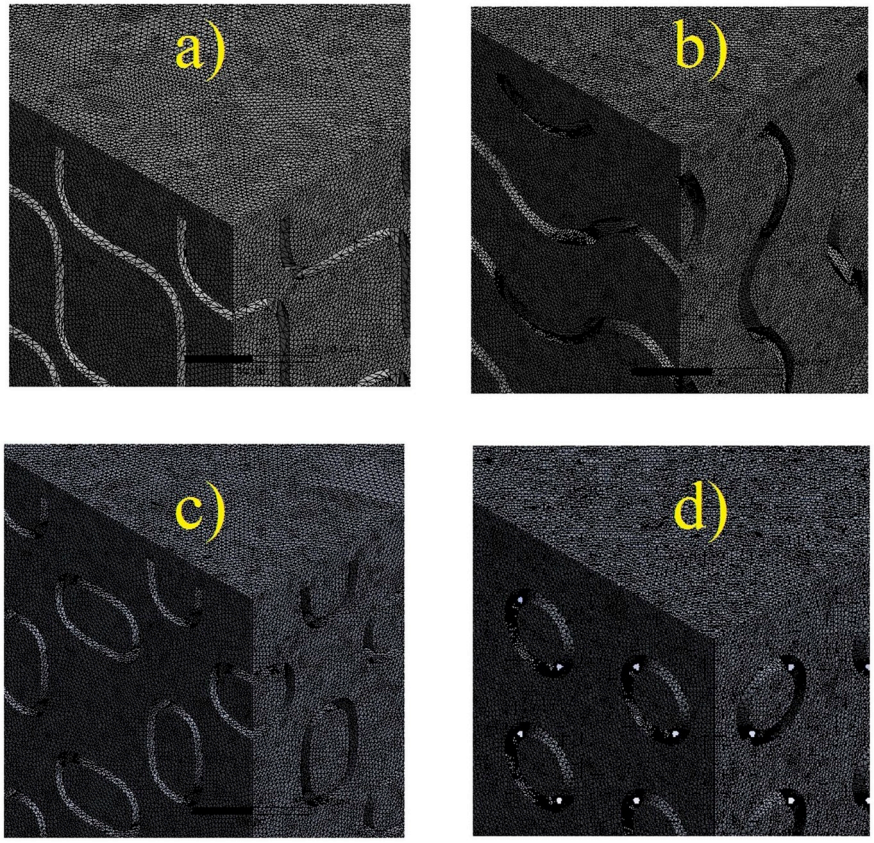

Fig. 2. Models were meshed using tetrahedral elements; a) double-diamond, b) gyroid, c) FR-D, and d) Schwarz-primitive.

Table 3
Reynold's number for any model for an inlet velocity of 0.001 m/s.

Model	Double-diamond	Gyroid	F-RD	Schwarz-primitive
Reynold's number	10.16	6.24	7.36	4.00

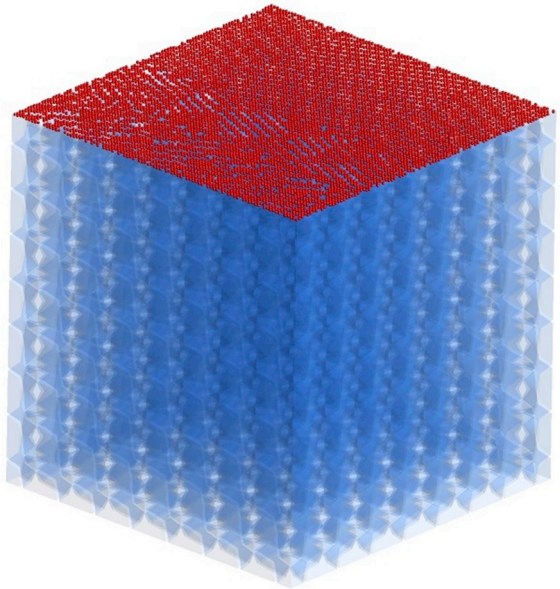

Fig. 3. Cells were injected from inlet surfaces.

compared with others; and the Schwarz-primitive model indicated the lowest amount.

Although the number of adhered cells was an important parameter in determining cell culturing efficiency, it did not designate the position and the modality of cell distribution within scaffolds. Cell distribution under inlet velocities of 0, 0.0001, 0.0005, and 0.0001 m/s was illustrated in Fig. 8.

3.5. Impact of culture media viscosity on cell sedimentation

Fluid flow-induced wall shear stress (WSS) is one of the most important stimuli in cell proliferation and differentiation during perfusion cell culture [42,43]; therefore, it should not be ignored. Although lower inlet velocity had increased cell attachment, its lower rate had significantly decreased WSS in all the models in this study (Fig. 9).

Although in CFD analysis of scaffolds for simplification the fluid was assumed to be water, but in practice it can possess higher viscosity than water. For example, Sinha et al. reported a media viscosity of 0.0037 Pa s with the addition of 5% wt/wt of dextran to water [44]. To determine cell culture media viscosity effect on cell deposition a viscosity of 0.0037 Pa s was selected and models were solved for an inlet velocity of 0.0001 m/s (Table 5).

With increasing viscosity, the number of trapped cells decreased significantly. Cell deposition amount, showed the lowest and highest sensitivity to the viscosity change in fluid phase in double-diamond and Schwarz-primitive models respectively.

4. Discussion

As can be seen, a large number of cells were agglomerated in the entrance regions in all the models for the inlet velocity of zero (static cell culture models). This meant that most of the cells in the absence of the fluid dragging force had been driven with the gravitational force

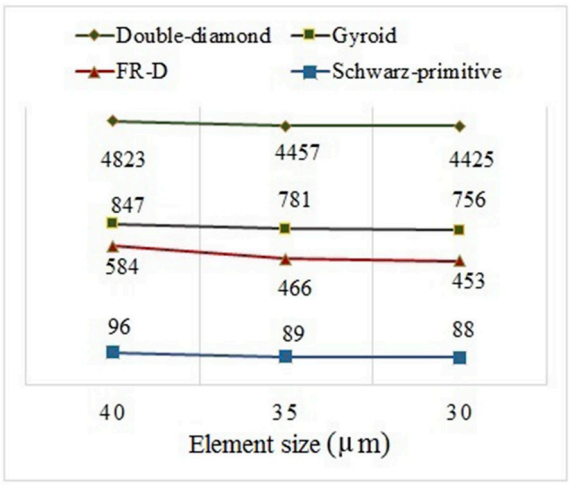

Fig. 4. Mesh size effect on trapped cells number in the models for an inlet velocity of 0.0001 m/s.

and downed vertically; then, they had been trapped as soon as they had hit any part of the scaffolds. For static cell culture conditions, a similar result had been also reported in Marin et al. work [18]. This phenomenon was not desirable, because the non-uniform distribution of the cells within the scaffolds could lead to heterogeneous tissue growth [31,45,46]. In terms of dynamic injection of cells, for all three velocities of 0.0001, 0.0005 and 0.001; the cells had relatively reached all regions of the scaffolds. This suggested that although the percentage of trapped cells was much less in dynamic cell culture than that in static ones, cell trapping by scaffolds had occurred more equally.

Among the models, the high-density distribution of cells was observed in the double-diamond model and the least dispersed cells were seen in Schwarz-primitive model for all inlet flow rates. For example, the percentage of sediment cells in the inlet velocity of 0.0001 m/s was 46% and 6.5% for the double-diamond and the Schwarz-primitive models respectively. This implied that the geometry of the scaffolds had affected cell seeding efficiency up to 7 times from architecture to architecture. The top view of the double-diamond model perspective showed no direct path for fluid flow from the inlet to the outlet, and the fluid had to flow through tortuous streamlines. The other models i.e. gyroid, F-RD, and Schwarz-primitive had sections that had allowed the fluid flow without colliding with any obstacle up to the outlet (Fig. 10).

In addition to the tortuosity, the changes in the cross-section of the scaffold microchannels were considered as other determinants affecting the number of trapped cells (Table 6).

As shown in Table 5, the lowest A/A_0 rate and the maximum.

D/d to other scaffolds in the double-diamond model had caused the largest number of adhered cells. Generally, a tortuous trajectory had increased the probability of cell collisions with the wall.

In addition to geometrical parameters and flow rate impacts on cell deposition amount in perfusion culture systems, the carrying fluid

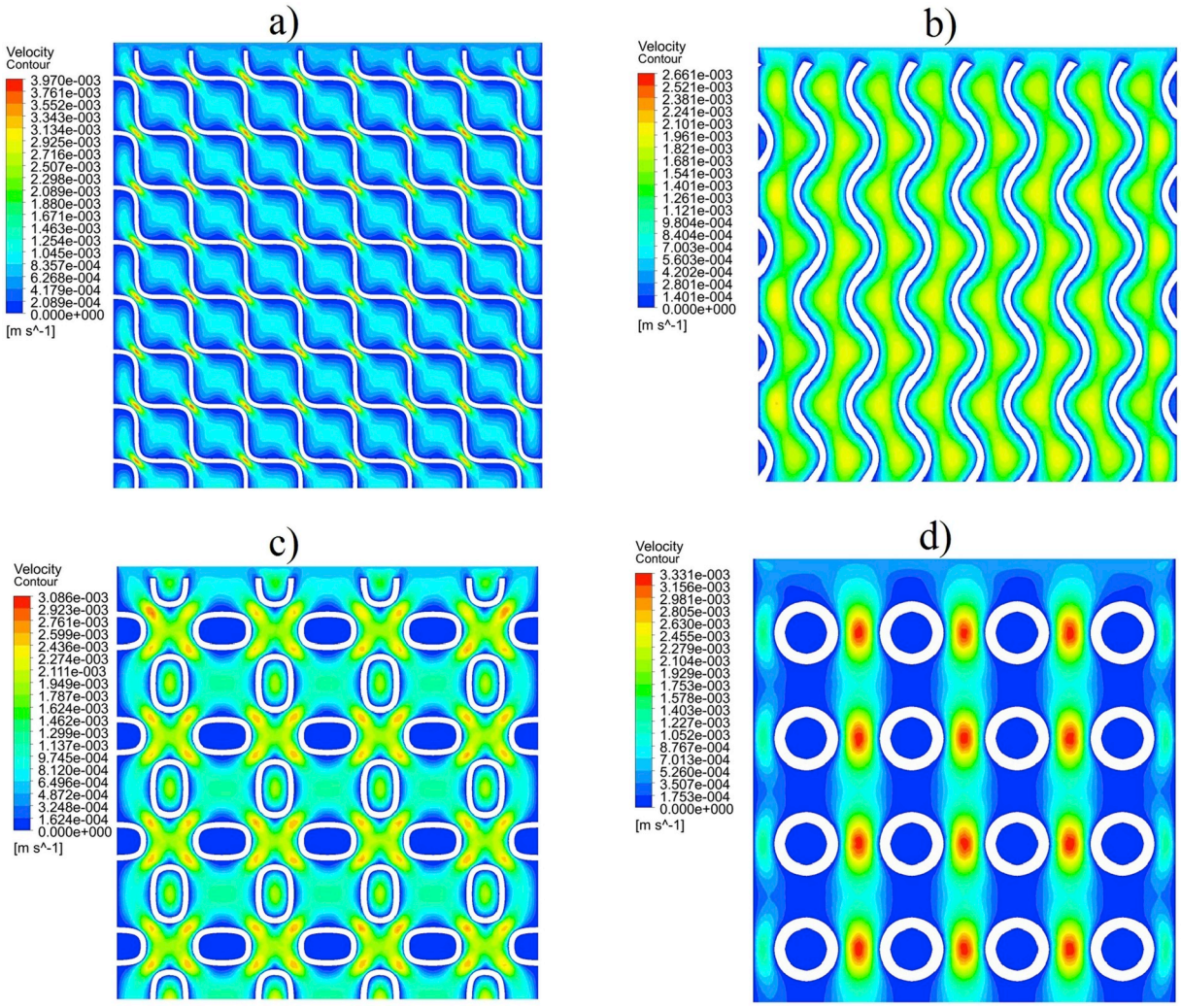

Fig. 5. Velocity contours in mid-section of the scaffolds for an inlet velocity of 0.0005 m/s; a) double-diamond, b) gyroid, c) FR-D, and d) Schwarz-primitive.

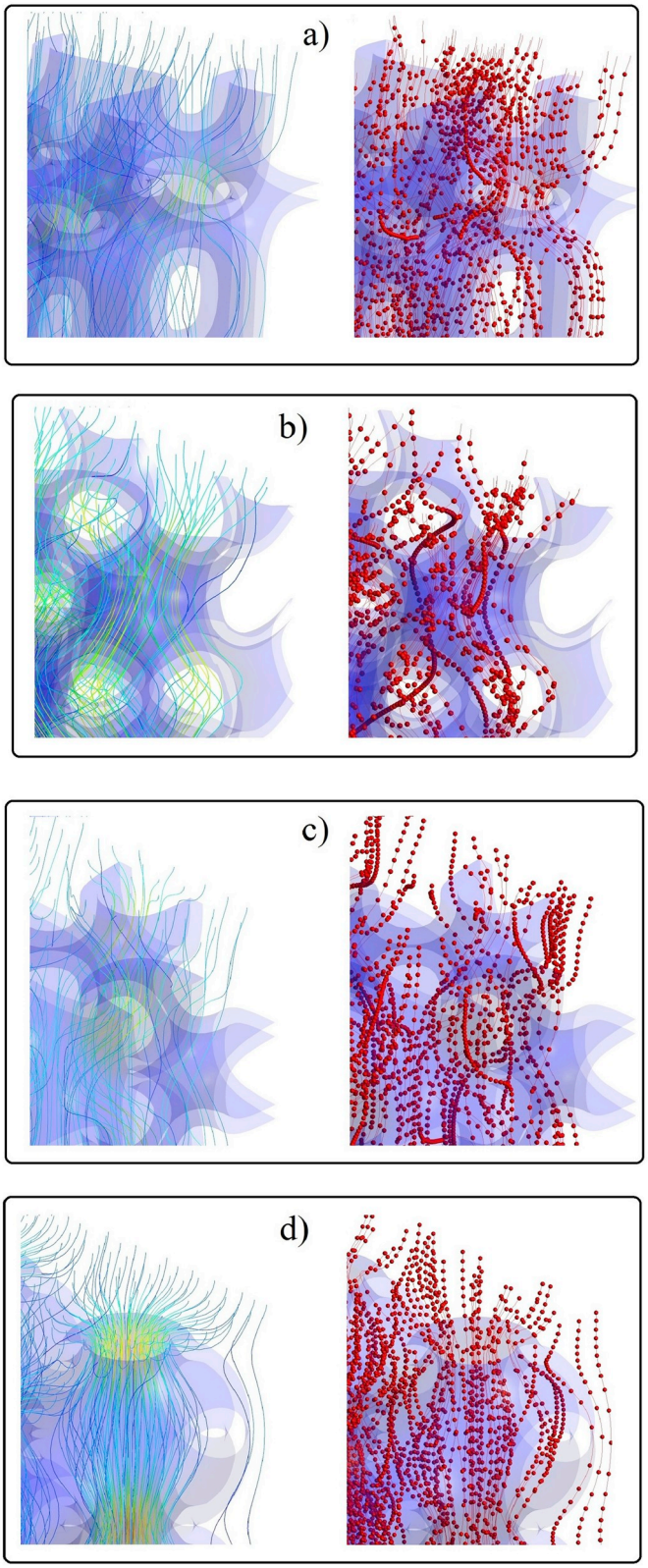

Fig. 6. Fluid velocity streamlines and cells trajectories in the models; a) double-diamond, b) gyroid, c) FR-D, and d) Schwarz-primitive.

viscosity impact on trapped cell number was probed. Higher viscosity significantly decreased the trapped cell number in all the models. This result is in good compliance with Momen-Heravi et al. work on microvesicles sedimentation in biofluid [47]. They showed increasing viscosity in biofluid led to less sedimentation of microvesicles. This phenomenon can be related to dragging force. With increasing viscosity, the dragging force of the fluid increases on the particles (equation (3)) where it becomes the dominant factor in cell movement and forced particles to follow the fluid domain streamlines with a minimum deviation. Where fluid streamlines can only touch scaffolds in the wall sections, it can be concluded that only cells presenting in boundaries can hit scaffolds and the rest of them leave the scaffolds microchannels without any contact.

Table 4
Number of adhered cells according to inlet velocity in each model.

Inlet velocity (m/s)	Number of trapped cells/whole injected cells			
	Double-diamond	Gyroid	F-RD	Schwarz-primitive
0.001	2118/10322	128/3893	163/5225	25/1600
0.0005	2423/10322	247/3893	211/5225	37/1600
0.0001	4425/10322	756/3893	453/5225	88/1600
0	10195/10322	2953/3893	4120/5225	962/1600

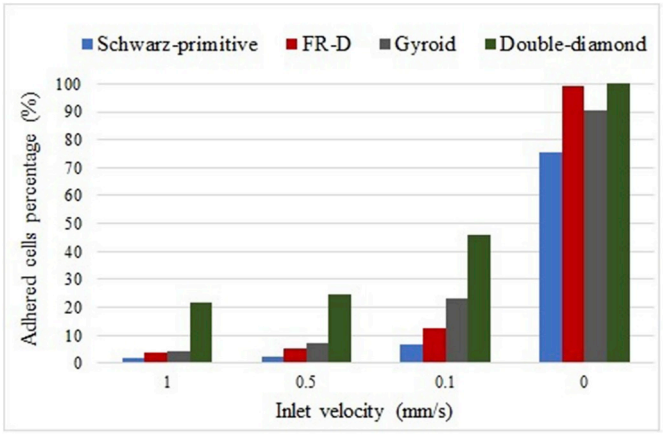

Fig. 7. Percentage of adhered cells in each model for different inlet velocities.

5. Conclusion

The purpose of this study was to investigate the effect of scaffold architecture on the number of trapped cells within porous scaffolds in a perfusion cell culture system. The results of this study could be summarized as follows:

- In a static cell culture system, more cells were trapped than those in dynamic culture models, but they were aggregated at the entrance regions of the scaffolds, which was known to be an undesirable phenomenon in cell culture process.
- With the same porosity, scaffold architecture could dramatically change cell seeding efficiency. For example, the double-diamond scaffold model trapped seven times more cells than the Schwarz-primitive model did in an inlet velocity of 0.1 mm/s in this study.
- Along with the scaffold architecture, the inlet velocity of perfusion culture also affected cell seeding efficiency, so that the number of trapped cells increased by three times through reducing the inlet velocity to 1/10.
- In addition to the geometric parameters and fluid inlet velocity, fluid viscosity was an important factor in determining the efficiency of cell culture that should be considered in the cell culture process.
- Although the results of this in silico analysis shed more light on the selection of scaffold architectures for cell culture, the overall conclusion in this domain required further investigations, especially experimental studies.

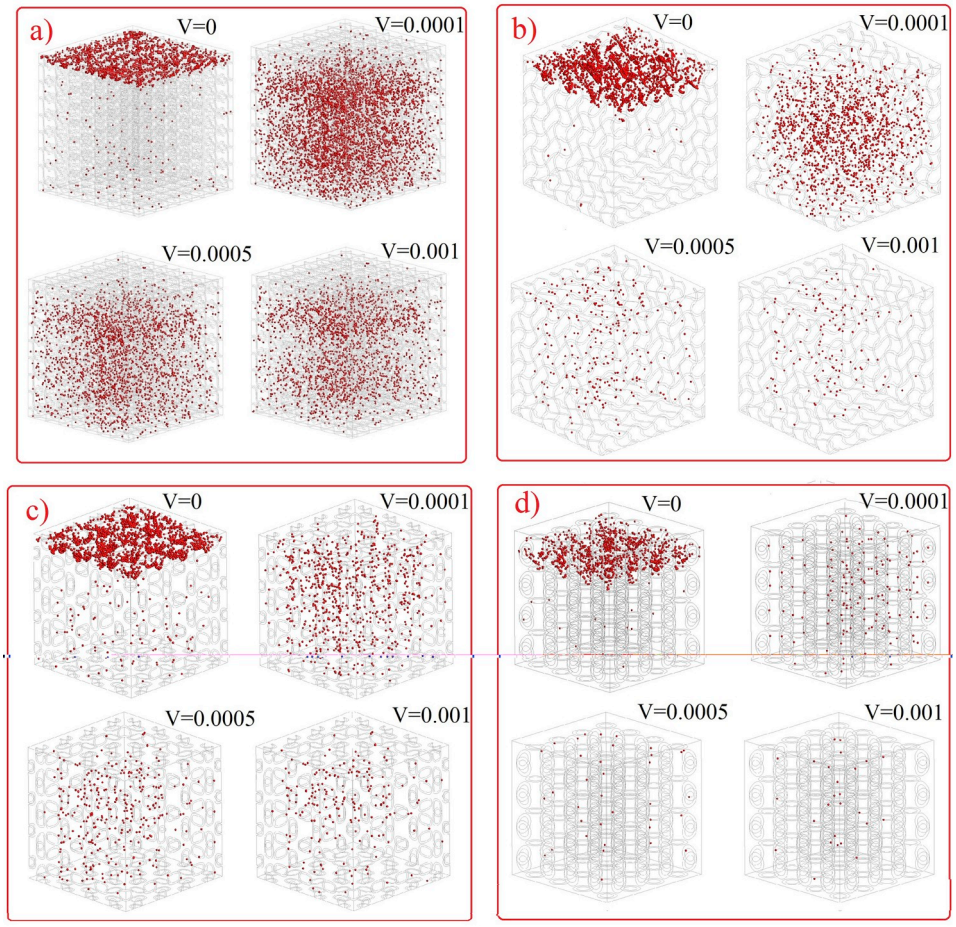

Fig. 8. Deposited cell distribution within a) double-diamond, b) gyroid, c) F-RD, and d) Schwarz-primitive models for different inlet velocities.

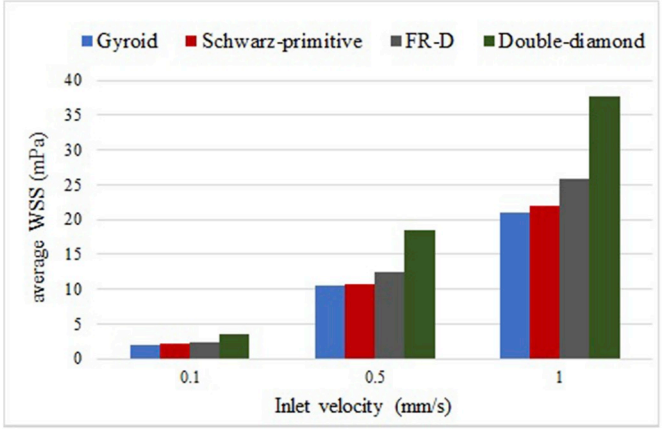

Fig. 9. Fluid flow-induced average WSS on scaffold walls for different inlet velocities.

Table 5
Effect of cell culture media viscosity on cell deposition amount at a perfusion velocity of 0.0001 m/s.

Viscosity (Pa.s)	Number of trapped cells/whole injected cells			
	Double-diamond	Gyroid	F-RD	Schwarz-primitive
0.0010	4425/10322	756/3893	453/5225	88/1600
0.0037	2820/10322	361/3893	279/5225	28/1600

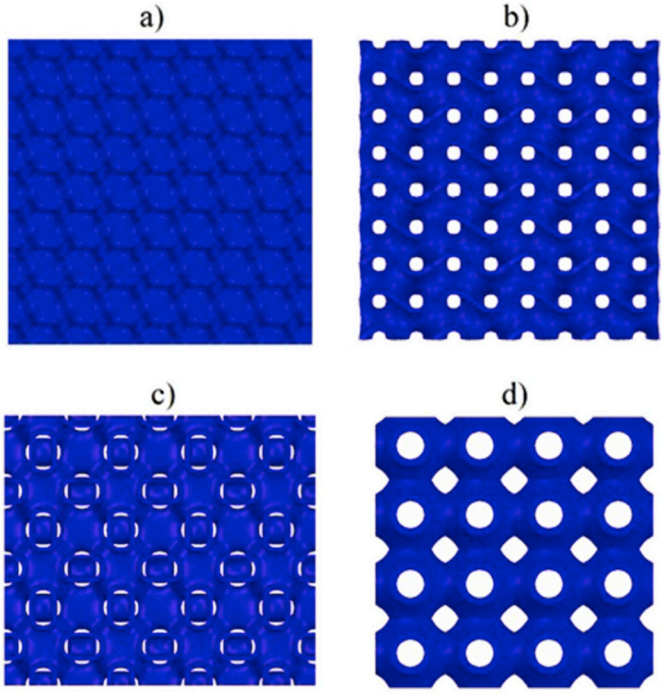

Fig. 10. Top views of a) double-diamond, b) gyroid, c) F-RD, and d) Schwarz-primitive models.

Table 6
Geometrical parameters of models; wherein A/A_0 and D/d respectively represented the ratio of the area with no obstacles to the total inlet area and the widest pore size to the narrowest one.

Model	Double-diamond	Gyroid	F-RD	Schwarz-primitive
A/A_0 (%)	0.00	10.63	4.80	21.50
D/d	5.88	1	3	2.27

Conflicts of interest

The author declare no conflicts of interest.

References

[1] H. Tavassoli, S.N. Alhosseini, A. Tay, P.P.Y. Chan, S.K. Weng Oh, M.E. Warkiani, Large-scale production of stem cells utilizing microcarriers: a biomaterials engineering perspective from academic research to commercialized products, Biomaterials 181 (2018) 333–346.

[2] E. Zermatten, J.R. Vetsch, D. Ruffoni, S. Hofmann, R. Müller, A. Steinfeld, Micro-computed tomography based computational fluid dynamics for the determination of shear stresses in scaffolds within a perfusion bioreactor, Ann. Biomed. Eng. 42 (2014) 1085–1094.

[3] I. Bružauskaitė, D. Bironaitė, E. Bagdonas, E. Bernotienė, Scaffolds and cells for tissue regeneration: different scaffold pore sizes-different cell effects, Cytotechnology 68 (2016) 355–369.

[4] Y. Mei, K. Saha, S.R. Bogatyrev, J. Yang, A.L. Hook, Z.I. Kalcioglu, S.-W. Cho, M. Mitalipova, N. Pyzocha, F. Rojas, K.J. Van Vliet, M.C. Davies, M.R. Alexander, R. Langer, R. Jaenisch, D.G. Anderson, Combinatorial development of biomaterials for clonal growth of human pluripotent stem cells, Nat. Mater. 9 (2010) 768.

[5] I.C. Lee, Y.T. Lee, B.Y. Yu, J.Y. Lai, T.H. Young, The behavior of mesenchymal Stem cells on micropatterned PLLA membranes, J. Biomed. Mater. Res. A 91A (2009) 929–938.

[6] R. Ayala, C. Zhang, D. Yang, Y. Hwang, A. Aung, S.S. Shroff, F.T. Arce, R. Lal, G. Arya, S. Varghese, Engineering the cell–material interface for controlling stem cell alialiadhesion, migration, and differentiation, Biomaterials 32 (2011) 3700–3711.

[7] P. Viswanathan, M.G. Ondeck, S. Chirasatitsin, K. Ngamkham, G.C. Reilly, A.J. Engler, G. Battaglia, 3D surface topology guides stem cell adhesion and differentiation, Biomaterials 52 (2015) 140–147.

[8] L. Ghasemi-Mobarakeh, M.P. Prabhakaran, L.L. Tian, E. Shamirzaei-Jeshvaghani, L. Dehghani, S. Ramakrishna, Structural properties of scaffolds: crucial parameters towards stem cells differentiation, World J. Stem Cell. 7 (2015) 728–744.

[9] C.M. Murphy, M.G. Haugh, F.J. O'Brien, The effect of mean pore size on cell attachment, proliferation and migration in collagen-glycosaminoglycan scaffolds for bone tissue engineering, Biomaterials 31 (2010) 461–466.

[10] F.P.W. Melchels, B. Tonnarelli, A.L. Olivares, I. Martin, D. Lacroix, J. Feijen, D.J. Wendt, D.W. Grijpma, The influence of the scaffold design on the distribution of adhering cells after perfusion cell seeding, Biomaterials 32 (2011) 2878–2884.

[11] S. Van Bael, Y.C. Chai, S. Truscello, M. Moesen, G. Kerckhofs, H. Van Oosterwyck, J.P. Kruth, J. Schrooten, The effect of pore geometry on the in vitro biological behavior of human periosteum-derived cells seeded on selective laser-melted Ti6Al4V bone scaffolds, Acta Biomater. 8 (2012) 2824–2834.

[12] X.G. Li, Y.K. Dai, T. Shen, C.Y. Gao, Induced migration of endothelial cells into 3D scaffolds by chemoattractants secreted by pro-inflammatory macrophages in situ, Regen. Biomater. 4 (2017) 139–148.

[13] A.L. Olivares, D. Lacroix, Simulation of cell seeding within a three-dimensional porous scaffold: a fluid-particle analysis, Tissue Eng. C Methods 18 (2012) 624–631.

[14] Y. Guyot, F.P. Luyten, J. Schrooten, I. Papantoniou, L. Geris, A three-dimensional computational fluid dynamics model of shear stress distribution during neotissue growth in a perfusion bioreactor, Biotechnol. Bioeng. 112 (2015) 2591–2600.

[15] T.J. Spencer, L.A. Hidalgo-Bastida, S.H. Cartmell, I. Halliday, C.M. Care, In silico multi-scale model of transport and dynamic seeding in a bone tissue engineering perfusion bioreactor, Biotechnol. Bioeng. 110 (2013) 1221–1230.

[16] A.A. Adebiyi, M.E. Taslim, K.D. Crawford, The use of computational fluid dynamic models for the optimization of cell seeding processes, Biomaterials 32 (2011) 8753–8770.

[17] D. Ali, S. Sen, Permeability and fluid flow-induced wall shear stress of bone tissue scaffolds: computational fluid dynamic analysis using Newtonian and non-Newtonian blood flow models, Comput. Biol. Med. 99 (2018) 201–208.

[18] A.C. Marin, T. Grossi, E. Bianchi, G. Dubini, D. Lacroix, μ-Particle tracking velocimetry and computational fluid dynamics study of cell seeding within a 3D porous scaffold, J. Mech. Behav. Biomed. Mater. 75 (2017) 463–469.

[19] A. Campos Marín, M. Brunelli, D. Lacroix, Flow perfusion rate modulates cell deposition onto scaffold substrate during cell seeding, Biomech. Model. Mechanobiol. 17 (3) (2017) 675–687.

[20] S.B.G. Blanquer, M. Werner, M. Hannula, S. Sharifi, G.P.R. Lajoinie, D. Eglin, J. Hyttinen, A.A. Poot, D.W. Grijpma, Surface curvature in triply-periodic minimal surface architectures as a distinct design parameter in preparing advanced tissue engineering scaffolds, Biofabrication 9 (2017).

[21] D. Ali, S. Sen, Finite element analysis of mechanical behavior, permeability and fluid induced wall shear stress of high porosity scaffolds with gyroid and lattice-based architectures, J. Mech. Behav. Biomed. Mater. 75 (2017) 262–270.

[22] A.L. Olivares, È. Marsal, J.A. Planell, D. Lacroix, Finite element study of scaffold architecture design and culture conditions for tissue engineering, Biomaterials 30 (2009) 6142–6149.

[23] F. Liu, Z. Mao, P. Zhang, D.Z. Zhang, J. Jiang, Z. Ma, Functionally graded porous scaffolds in multiple patterns: new design method, physical and mechanical properties, Mater. Des. 160 (2018) 849–860.

[24] D. Ali, S. Sen, Computational fluid dynamics study of the effects of surface roughness on permeability and fluid flow-induced wall shear stress in scaffolds, Ann. Biomed. Eng. 46 (2018) 2023–2035.

[25] M. Rittman, M. Frischherz, F. Burgmann, P.G. Hartley, A. Squires, Direct visualisation of lipid bilayer cubic phases using Atomic Force microscopy, Soft Matter 6 (2010) 4058–4061.

[26] D.-J. Yoo, Computer-aided porous scaffold design for tissue engineering using triply periodic minimal surfaces, Int. J. Precis. Eng. Manuf. 12 (2011) 61–71.

[27] H.G. Lee, J. Kim, Regularized Dirac delta functions for phase field models, Int. J. Numer. Methods Eng. 91 (2012) 269–288.

[28] J.J. Brandner, E. Hansjosten, E. Anurjew, W. Pfleging, K. Schubert, Microstructure devices generation by selective laser melting - art. no. 645911, in: W. Pfleging, Y. Lu, K. Washio, F.G. Bachmann, W. Hoving (Eds.), Laser-based Micro- and Nanopackaging and Assembly, Spie-Int Soc Optical Engineering, Bellingham, 200745911-45911.

[29] X.B. Su, Y.Q. Yang, D.M. Xiao, Z.Y. Luo, An investigation into direct fabrication of fine-structured components by selective laser melting, Int. J. Adv. Manuf. Technol. 64 (2013) 1231–1238.

[30] P. Vossenberg, G.A. Higuera, G. van Straten, C.A. van Blitterswijk, A.J.B. van Boxtel, Darcian permeability constant as indicator for shear stresses in regular scaffold systems for tissue engineering, Biomech. Model. Mechanobiol. 8 (2009) 499.

[31] A.C. Marin, D. Lacroix, The inter-sample structural variability of regular tissue-engineered scaffolds significantly affects the micromechanical local cell environment, Interfac. Focus 5 (2015) 8.

[32] X. Xue, M.K. Patel, M. Kersaudy-Kerhoas, M.P.Y. Desmulliez, C. Bailey, D. Topham, Analysis of fluid separation in microfluidic T-channels, Appl. Math. Model. 36 (2012) 743–755.

[33] S.A. Morsi, A.J. Alexander, An investigation of particle trajectories in two-phase flow systems, J. Fluid Mech. 55 (1972) 193–208.

[34] A.K. Bryan, V.C. Hecht, W.J. Shen, K. Payer, W.H. Grover, S.R. Manalis, Measuring single cell mass, volume, and density with dual suspended microchannel resonators, Lab Chip 14 (2014) 569–576.

[35] S. Truscello, G. Kerckhofs, S. Van Bael, G. Pyka, J. Schrooten, H. Van Oosterwyck, Prediction of permeability of regular scaffolds for skeletal tissue engineering: a combined computational and experimental study, Acta Biomater. 8 (2012) 1648–1658.

[36] M. Pilou, S. Tsangaris, P. Neofytou, C. Housiadas, Y. Drossinos, Inertial particle deposition in a 90 degrees laminar flow bend: an eulerian fluid particle approach, Aerosol Sci. Technol. 45 (2011) 1376–1387.

[37] Y.S. Cheng, H.C. Yeh, M.D. Allen, Dynamic shape factor of a plate-like particle, Aerosol Sci. Technol. 8 (1988) 109–123.

[38] S. Gómez, M.D. Vlad, J. López, E. Fernández, Design and properties of 3D scaffolds for bone tissue engineering, Acta Biomater. 42 (2016) 341–350.

[39] S. Sohrabi, J.D. Zheng, E.A. Finol, Y.L. Liu, Numerical simulation of particle transport and deposition in the pulmonary vasculature, J. Biomech. Eng. Trans. ASME 136 (2014).

[40] F. Zhao, T. Ma, Perfusion bioreactor system for human mesenchymal stem cell tissue engineering: dynamic cell seeding and construct development, Biotechnol. Bioeng. 91 (2005) 482–493.

[41] D.O. Frank-Ito, M. Wofford, J.D. Schroeter, J.S. Kimbell, Influence of mesh density on airflow and particle deposition in sinonasal airway modeling, J. Aerosol Med. Pulm. Drug Deliv. 29 (2016) 46–56.

[42] R. Voronov, S. VanGordon, V.I. Sikavitsas, D.V. Papavassiliou, Computational modeling of flow-induced shear stresses within 3D salt-leached porous scaffolds imaged via micro-CT, J. Biomech. 43 (2010) 1279–1286.

[43] S. Ding, P. Kingshott, H. Thissen, M. Pera, P.Y. Wang, Modulation of human mesenchymal and pluripotent stem cell behavior using biophysical and biochemical cues: a review, Biotechnol. Bioeng. 114 (2017) 260–280.

[44] R. Sinha, S. Le Gac, N. Verdonschot, A. van den Berg, B. Koopman, J. Rouwkema, Endothelial cell alignment as a result of anisotropic strain and flow induced shear stress combinations, Sci. Rep. 6 (2016).

[45] A. Lesman, Y. Blinder, S. Levenberg, Modeling of flow-induced shear stress applied on 3D cellular scaffolds: implications for vascular tissue engineering, Biotechnol. Bioeng. 105 (2010) 645–654.

[46] D. Egger, M. Fischer, A. Clementi, V. Ribitsch, J. Hansmann, C. Kasper, Development and characterization of a parallelizable perfusion bioreactor for 3D cell culture, Bioengineering 4 (2017) 51.

[47] F. Momen-Heravi, L. Balaj, S. Alian, A.J. Trachtenberg, F.H. Hochberg, J. Skog, W.P. Kuo, Impact of biofluid viscosity on size and sedimentation efficiency of the isolated microvesicles, Front. Physiol. 3 (2012).